# NJC

Accepted Manuscript


This is an *Accepted Manuscript*, which has been through the Royal Society of Chemistry peer review process and has been accepted for publication.

*Accepted Manuscripts* are published online shortly after acceptance, before technical editing, formatting and proof reading. Using this free service, authors can make their results available to the community, in citable form, before we publish the edited article. We will replace this *Accepted Manuscript* with the edited and formatted *Advance Article* as soon as it is available.

You can find more information about *Accepted Manuscripts* in the Information for Authors.

Please note that technical editing may introduce minor changes to the text and/or graphics, which may alter content. The journal's standard Terms & Conditions and the Ethical guidelines still apply. In no event shall the Royal Society of Chemistry be held responsible for any errors or omissions in this *Accepted Manuscript* or any consequences arising from the use of any information it contains.

ROYAL SOCIETY OF CHEMISTRY

www.rsc.org/njc

Journal Name

RSCPublishing

ARTICLE

# Templating synthesis of metal oxides by an incipient wetness impregnation route and their activities for CO oxidation

Cite this: DOI: 10.1039/xoxxoooooox

Received ooth January 2012,
Accepted ooth January 2012

DOI: 10.1039/xoxxoooooox

www.rsc.org/

Haifeng Gong, Junjiang Zhu*, Kangle Lv, Ping Xiao, Yanxi Zhao*

Various metal oxides, including $Co_3O_4$, NiO, $CeO_2$ and $Ce_{0.7}Cu_{0.3}O_2$, were synthesized by an incipient wetness impregnation (IWI) route using mesoporous silica SBA-16 and SBA-15 as template, and their catalytic performances were evaluated by the CO oxidation model reaction. Templating is a powerful technology for the preparation of materials with desired morphology, while the IWI route guarantees the metal in solution permeating into the pores of template by a capillary pressure. Thus mesoporous metal oxides with near-perfect surface morphologies, such as three dimensional nano-sized particles and two dimensional nanowires, and controlled particle size were prepared from shaped templates with the IWI route. Characterizations such as TEM and $H_2$-TPR measurements indicate that $Co_3O_4$ replicated from SBA-16 hydrolyzed at 80 °C ($Co_3O_4$-16_80) has the smallest particle size, the highest surface area and the strongest reducibility, thus leading to the best activity for CO oxidation. Furthermore, the replicated $Co_3O_4$-16_80 can be reused with no loss of activity in the second run, and has good long-term stability, with less than 6% decrease in the activity after running at 120 °C for 36 h.

## 1. Introduction

Since the pioneering work of Kresge et al,[1] mesoporous materials have received tremendous attentions in many fields including catalysis, sorption, gas sensors, and optics, due to the attractive properties resulted from their high surface area, nano crystallinity, mesoporosity, and pore volume, relative to that of the nonporous counterparts.[2-4] Among them, the synthesis of mesoporous transition metal oxides with controlled surface morphology is especially interesting because of their lost-cost, active surface chemistries and widely industrial applications.

Templating is an effective method for the synthesis of mesoporous metal oxides, using either surfactant micelles (e.g., P123) or shaped materials (e.g., mesoporous silica) as template. The templating by surfactant micelles generally is more difficult because the surfactant/oxide composite precursors are often susceptible to lack of condensation, redox reactions, or phase transitions accompanied by thermal breakdown of the structural integrity.[5,6]

The templating by shaped materials, which is so-called hard template method and is initiated by the group of prof. Ryoo for the synthesis of ordered mesoporous carbon,[7] is an attractive route for the preparation of mesoporous metal oxides.[8-13] In this method, soluble metal salts are used as precursors and their permeation to the pores of template is a crucial step. Indeed, it is reported that in the nanocasting method the metal precursor (e.g., $Co(NO_3)_3{\bullet}6H_2O$) has to be impregnated several times in order to increase the loading and improve the yield.[11,14,15] To simplify the impregnation process while achieving high yields, various strategies were developed, such as the "bisolvent" impregnation method in which co-solvent is used to improve the accessibility of metal nitrates to the pores of template,[16, 17] and the solid-liquid method in which the metal precursor was heated to its melting temperature and then entered the pores of template by a capillary action.[18, 19] Also, assistant technologies such as ultrasonic irradiation, refluxing and vacuum-pumping are reported to be effective in promoting the access of metal nitrate to the pores of template.[20-23]

On the other hand, strict legislations on environmental protection issued in recent decades impel the scientist to find solutions for removing pollutants emitted to the environment. Catalysis is a good means in this respect and has been proven to be effective in practice. For example, the removal of pollutant CO emitted from exhaust is normally conducted by a catalytic oxidation route, and mesoporous metal oxides are reported to be active for the reaction.[24-28] Cobalt-containing materials receive special interest in this reaction because of its rather high activity relative to that of other metal-containing catalysts,[29-31] and it is believed that the catalytic performances of $Co_3O_4$, for example, for CO oxidation depend intimately on the crystal sizes, morphologies, and exposed crystal facets.[32-36] Hence, the preparation of mesoporous metal oxides with desired sizes and morphologies would be of interest for catalysis use.

Herein we reported the preparation of mesoporous transition metal oxides by a templating method with an incipient wetness impregnation (IWI) route, and their catalytic performances for CO oxidation were evaluated. The IWI is an effective method for the preparation of supported noble metal[37-39] or metal oxide catalysts,[40-42] by which the metal precursors can be effectively

permeated into the pores of support by capillary pressure, while CO oxidation is not only a main route of removing CO pollutant but also a widely used model reaction to evaluate the catalytic performances of materials. Results indicated that mesoporous metal oxide with uniform particle size and pores can be replicated from the template, and the particle size and the surface morphology depend intimately on those of the template. Both simple and complex metal oxide (e.g., $Co_3O_4$, NiO, $CeO_2$ and $Ce_{0.7}Cu_{0.3}O_2$) were synthesized. The prepared metal oxides, $Co_3O_4$ for example, show high activity and good stability for CO oxidation, with about 80% activity at 120 °C and no loss of activity is observed in the second run, and less than 6% decrease in the activity after working at 120 °C for 6 h.

## 2. Experimental

### 2.1 Synthesis of mesoporousSBA-16 and SBA-15

Ordered mesoporous silica SBA-16 and SBA-15 were prepared according to reported procedures.[43-45] P123 and/or F127, de-ionized water and 2 M HCl were mixed and stirred at 35 °C. After P123/F127 was completely dissolved, tetraethyl orthosilicate (TEOS) were added dropwise and stirred for 24 h. Thereafter, the solution was transferred to an autoclave and aged at 80-120 °C for another 24 h. The sample was filtered, dried at 100 °C overnight and finally calcined in an air oven at 550 °C for 6 h with a heating rate of 2 °C $min^{-1}$. For SBA-15, the hydrothermal temperature was set at 100 °C; For SBA-16, the hydrothermal temperature was controlled at 80, 100 or 120 °C in order to get samples with different texture structures (e.g., surface area, pore size and pore volume). The obtained samples were denoted as SBA-n_T, where "n" represents the number (15 or 16) and "T" represents the hydrothermal temperature (80, 100 or 120).

### 2.2 Synthesis of mesoporous $Co_3O_4$

Typically, 1.23 g $Co(NO_3)_2$•$6H_2O$ was firstly dissolved in 2 mL deionized water, and then added dropwise to 1 g template (SBA-16_T and SBA-15_100) pre-treated at 100 °C for 24 h. The mixture was stirred with a spatula for several minutes to ensure that the solution is homogeneously dispersed on the template. The resulting sample was dried in an air oven at 100 °C overnight to evaporate the water, and then calcined at 450 °C for 6 h with a heating rate of 2°C $min^{-1}$, to yield $Co_3O_4$-silica composites. The loading of $Co_3O_4$ was 25% in weight. It should be noted that this strategy is different from that reported in literature, where excessed volume of metal solution is used and the impregnation is conducted by adding the template to metal solution. Thus high yield of metal oxides can be obtained without repeating the impregnation step in the current method.

To prepare mesoporous $Co_3O_4$, the obtained $Co_3O_4$/SBA-16 composites were treated with 50 mL 4 M $NH_4HF_2$ at room temperature for 48 h to etch the silica template, as that widely used in literature. The resulting suspension was centrifuged and the solid at the bottom was then separated and dried at 60 °C for 5 h. Based on the nomenclature of templates, the samples were denoted as $Co_3O_4$-n_T. Other mesoporous metal oxides (NiO, $CeO_2$ and $Ce_{0.7}Cu_{0.3}O_2$) were prepared with the same procedures, using the corresponding metal nitrate.

For comparison, an extra $Co_3O_4$ was prepared by a sol-gel method, details of which was described in a previous work[46] and it was denoted $Co_3O_4$-EG.

### 2.3 Characterizations

X-Ray diffraction (XRD) patterns were collected using a Bruker D8 Advance X-ray diffractometer with Cu Kα (λ = 1.5406 Å) irradiation, operated at voltage of 40 kV and applied potential current of 40 mA. The 2θ angle ranged from 0.5 to 5° and 10 to 80° for the small-angle and wide-angle XRD, with scanning speed of 0.6° $min^{-1}$ and 10° $min^{-1}$, respectively.

Transmission electron microscopy (TEM) images were obtained on a Tecnai $G^2$ 20 S-Twin apparatus. The sample was first ultrasounded in ethanol for several seconds, and then depositing on a copper mesh for observation.

Field-emission scanning electron microscopy (FESEM) images were observed on an SU8000 apparatus (Hitachi, Japan), with an accelerating voltage of 15 kV.

$N_2$ physisorption isotherms were measured on a Quanta-chrome Autosorb-1-C apparatus at liquid nitrogen temperature (-196 °C) and the surface area was calculated using the Brunauer–Emmett–Teller method. Before measurement the sample was treated in vacuum at 200 °C for 5 h.

X-ray photoelectron spectroscopy (XPS) spectra were recorded on a Thermo Electron Corporation VG Multilab 2000 apparatus using a monochromatic Al Ka X-ray source (300 W) and analyzer pass energy of 25 eV. Binding energies were obtained by referencing to the C (1s) binding energy of carbon taken at 284.6 eV.

Temperature-programmed reduction of $H_2$ ($H_2$-TPR) was performed on a FINESORB-3010 apparatus (Zhejiang Fantai instrument company, China). The sample (30 mg) was first treated in $O_2$ at 500 °C for 1 h and then cooled to room temperature. Thereafter 5 vol.% $H_2/N_2$ mixture with flow rate of 20 mL $min^{-1}$ was switched on. After reaching a stable baseline the sample was heated from RT to 800 °C at a rate of 10 °C $min^{-1}$ to record the profile.

### 2.4 Catalytic tests

Catalytic tests were performed on a continuous flow fixed-bed quartz microreactor (i.d. = 8 mm) equipped with a temperature programmed controller at atmospheric pressure. 50 mg catalyst was loaded into the microreactor without dilution. The reactant 0.5% CO + 7.5% $O_2$ + 92% Ar was passed at a flow rate of 50 mL $min^{-1}$, corresponding to a space velocity of 60,000 mL $g^{-1}$ $h^{-1}$. The effluent gases were analyzed by an on-line GC (Agilent 7890) equipped with a thermal conductivity detector and two packed columns (Porapak Q and 5A molecular sieve). CO oxidation activity was evaluated in terms of CO conversion: % Conversion = $[(CO)_{in} - (CO)_{out}]/(CO)_{in} * 100$, where $(CO)_{in}$ and $(CO)_{out}$ represent the inlet and outlet concentration of CO, respectively.

## 3. Results and Discussion

The mesoporous metal oxides (e.g., $Co_3O_4$) studied here were prepared by a templating method using ordered mesoporous silica SBA-15 and SBA-16 hydrolysed at varied temperatures as templates. Catalytic performances of metal oxides replicated from the templates were then tested by the CO oxidation model reaction, to optimize the preparation condition and see their potential application in practice. To confirm that metal oxides with desired crystalline and textural structure were prepared, and studied their physicochemical properties, a series of characterizations were applied, including wide- and small-XRD, $N_2$ physisorption, TEM, SEM, XPS and $H_2$-TPR, as below.



 

### 3.1 Crystalline and textural structure

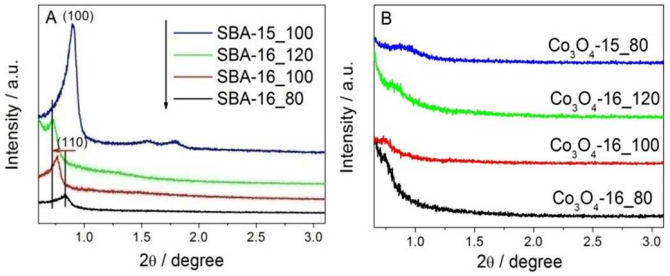


Figure 1. Small-angle XRD patterns for (A) the ordered mesoporous silica templates and (B) the replicated $Co_3O_4$-16_T and $Co_3O_4$-15_100.

Figure 1A shows the small-angle XRD diffraction patterns of SBA-15_100 and SBA-16-T. A well resolved diffraction peak, corresponding to the (100) face of SBA-15 or the (110) face of SBA-16, is observed for the samples, in agreement with the reported results.[47, 48] Although the peak intensity of SBA-16 is weak, which makes it not sufficient to prove directly the exact structure of SBA-16, the supplementary measurements such as $N_2$ physisorption and TEM confirm it (see below). In addition, it is seen that for SBA-16_T, the position of (110) peak shifts to lower 2θ angle and the intensity strengthens gradually with the temperature, indicating that the hydrothermal temperature has significant influences on the textural structure of SBA-16. The lower peak position and the stronger peak intensity indicate that SBA-16_T with enlarged interplanar spacing and higher degree of long-range order of channels is obtained at higher temperature.

Unfortunately, no defined diffraction peak, but rather diffuse scattering, is observed in the small-angle XRD patterns for the replicated $Co_3O_4$, Figure 1B. This could be that the $Co_3O_4$ is in disordered structure or that the long-range order of channels of porous $Co_3O_4$ is damaged during the template leaching process. To clarify this, in the following we conducted $N_2$ physisorption and TEM measurements, which show that the samples have an ordered structure. Therefore, the unseen diffraction peak should be the reason that the long-range order of channels of $Co_3O_4$ is damaged. Indeed, we can see that even for the SBA-16 template, the peak intensity is rather weak (relative to that of SBA-15). It is thus acceptable that no appreciated diffraction peak appears for the replicated $Co_3O_4$. The small-angle XRD diffraction peak of other metal oxides including NiO, $CeO_2$ and $Ce_{0.7}Cu_{0.3}O_2$ is also weak, see Figure S1, but has an ordered structure like the SBA-15 template, as evidenced from TEM images (Figure S4).

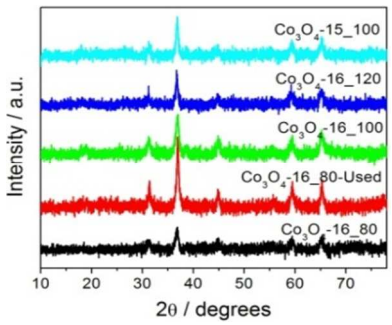


Figure 2. Wide-angle XRD patterns for the replicated $Co_3O_4$-16_T and $Co_3O_4$-15_100, and the used $Co_3O_4$-16_80 ($Co_3O_4$-16_80-Used).

The wide-angle XRD patterns reveal that face centered cubic $Co_3O_4$ (JCPDS Card No. 42-1467) is replicated when the cobalt oxides/silica composites is calcined at 450 °C, Figure 2. The weak peak intensity could be attributed to its small particle size. The crystalline size (C.S.), calculated from the line broadening of the $d_{311}$ reflection peak of $Co_3O_4$ (2θ = 36.7°) using the Scherrer equation, increases in order of $Co_3O_4$-16_80 < $Co_3O_4$-16_100 < $Co_3O_4$-16_120, Table 1. This can be attributed to the increased pore size of SBA-16_T from 80 to 100 and to 120 °C (Figure S2), as larger pore allows more metal solutions to enter, forming larger particle size. It should be noted that the C.S. of $Co_3O_4$ is a bit larger than the pore size of SBA-16, which could be that 1) the calculated C.S. is not accurate due to the weak peak intensity and peak broadening, and 2) a different working principle between these two measurements. The $Co_3O_4$-15_100 replicated from SBA-15 shows identical XRD diffractions to that from SBA-16, and the crystalline size is 20.4 nm.

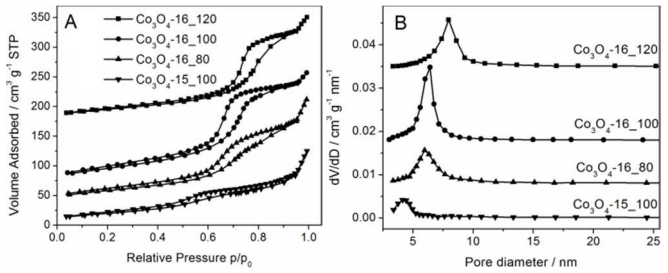


Figure 3. (A) $N_2$ adsorption–desorption isotherms and (B) pore size distributions of the replicated $Co_3O_4$-16_T and $Co_3O_4$-15_100. Note: the curves were shifted down or up for clearness.

Figure 3 presents the $N_2$ adsorption-desorption isotherms and pore size distributions of the replicated $Co_3O_4$-16_T and $Co_3O_4$-15_100, showing a typical type-IV isotherm with a H1-type hysteresis loop, which is similar to that of the template SBA-16 (Figure S2) and is characteristic of mesoporous materials.[19] This confirms that mesoporous $Co_3O_4$ is replicated from the template, and is comparable to the replication of mesoporous carbon (CMK-3) reported in literature.[7, 49]

Table 1.Structural parameters of the replicated mesoporous $Co_3O_4$ samples

| Catalyst | C. S. (nm) [a] | $S_{BET}$ ($m^2/g$) [b] | P.V.[c] /$cm^3$ $g^{-1}$ | $D_{BJH}$[d] / nm |
|---|---|---|---|---|
| $Co_3O_4$-16_120 | 23.5 | 90.2 | 0.28 | 8.0 |
| $Co_3O_4$-16_100 | 19.2 | 100.8 | 0.29 | 6.4 |
| $Co_3O_4$-16_80 | 16.1 | 130.1 | 0.31 | 6.0 |
| $Co_3O_4$-15_100 | 20.4 | 73.5 | 0.19 | 4.1 |

[a]Crystallite size calculated from XRD patterns by the Scherrer equation; [b]BET specific surface area; [c]Total pore volume; [d]Pore diameter calculated by the desorption branch of isotherms using the BJH method.

The textural properties of the replicated mesoporous $Co_3O_4$ are listed in Table 1. As expected, the surface area and the pore volume increase, and the pore size decreases from $Co_3O_4$-16_120 to $Co_3O_4$-16_100 and to $Co_3O_4$-16_80, in accordance to the changes observed for SBA-16_T, confirming that $Co_3O_4$-16_T is replicated from the template. By comparison, the replicated $Co_3O_4$-15_100 shows the lowest surface area (73.52 $m^2g^{-1}$), pore volume (0.186 $cm^3g^{-1}$) and pore size (4.13 nm), which could be attributed to its nanowire structure (see TEM images below).

### 3.2 Surface morphologies

Figure 4 shows the TEM images of $Co_3O_4$-16_T and $Co_3O_4$-15_100 after etching the silica template by 4M $NH_4HF_2$, and

these of the templates are shown in Figure S3. The morphology of $Co_3O_4$ depends closely on that of the template, thus $Co_3O_4$-16_T replicated from cage-structured SBA-16 are entities with three-dimensionally (3D) ordered structure, and $Co_3O_4$-15_100 replicated from channel-structured SBA-15 are nanowires with 2D ordered structure. Similarly, other metal oxides including NiO, $CeO_2$ and $Ce_{0.7}Cu_{0.3}O_2$ with nanowires structure are replicated when SBA-15 was used as template, Figure S4, supporting the above conclusions that metal oxides with desired morphology can be obtained using a shaped template.

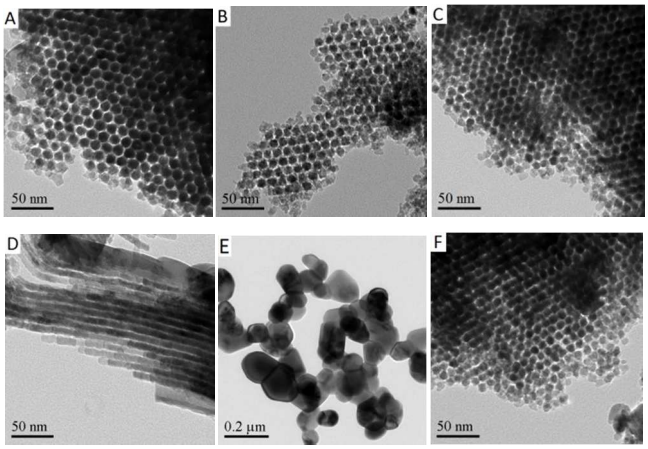


Figure 4. TEM images of (A) $Co_3O_4$-16_120, (B) $Co_3O_4$-16_100, (C) $Co_3O_4$-16_80, (D) $Co_3O_4$-15_100, (E) $Co_3O_4$-EG and (F) the used $Co_3O_4$-16_80 ($Co_3O_4$-16_80-Used).

For comparison, TEM image of $Co_3O_4$-EG prepared by sol-gel method using ethylene glycol and methanol as solvents was also taken, Figure 4E, showing that the sample is composed of large particles with randomly arranged structure and the particle size is widely distributed. Obviously, none ordered structure could be formed if no template is used. It is interesting to find, however, that the particles are connected one by one, and interstitial pores are formed, suggesting that the sample could also be an attractive material for catalysis use.

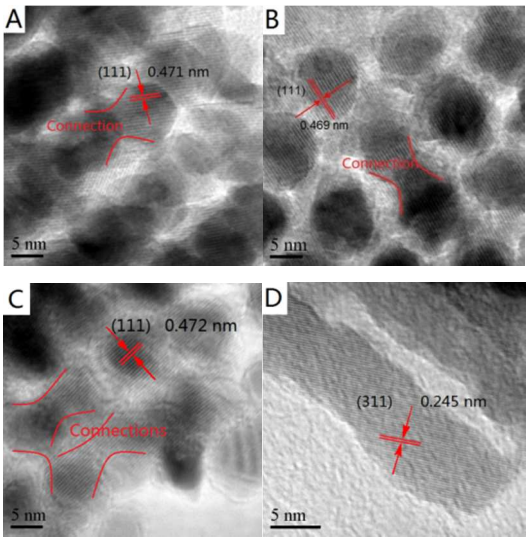


Figure 5. HRTEM images of the replicated $Co_3O_4$: (A) $Co_3O_4$-16_120, (B) $Co_3O_4$-16_100, (C) $Co_3O_4$-16_80 and (D) $Co_3O_4$-15_100.

High resolution TEM (HRTEM) images are taken to see the detailed structure and the particle size of the replicated $Co_3O_4$ samples, Figure 5. Lattice fringes are clearly observed for all the samples, indicating a well crystalline structure. On the other hand, it is seen that the particles are connected with each other for $Co_3O_4$-16_T, forming a net structure. The presence of this connection indicates that the $Co_3O_4$ in the pores, which are used to link the cages of SBA-16, is also replicated. Because of these connections, the replicated $Co_3O_4$ particles are connected with each other and remain the ordered pore structure of SBA-16, as seen from Figure 4A-4C. Similarly, the channel structure of SBA-15 is also replicated by the sample $Co_3O_4$-15_100.

As expected, the domain particle size of $Co_3O_4$ increases as the pores of SBA-16, in order of $Co_3O_4$-16_80 < $Co_3O_4$-16_100 < $Co_3O_4$-16_120, with the value increased from 10.2 to 13.1 and to 15.4 nm, indicating that $Co_3O_4$-16_T is well replicated from SBA-16_T. The diameter of $Co_3O_4$-15_100 is measured to be 9.0 nm, which fits well to the pore diameter (9.5 nm) of the parent SBA-15-100, determined using the BJH algorithm from the desorption branch of the $N_2$ physisorption isotherm.[50]

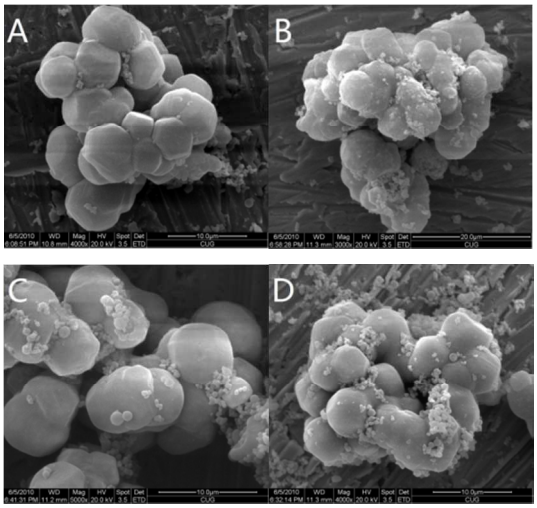


Figure 6. SEM images of $Co_3O_4$/SBA-16_100 with $Co_3O_4$ loading of (A) 10 wt.%, (B) 20 wt.%, (C) 30 wt.% and (D) 40 wt.%.

As indicated at the beginning, the permeation of metal precursors to the pores of template is an important parameter of the template method which may affect the yield of replicate. For this, we synthesized $Co_3O_4$/SBA-16_100 composites with $Co_3O_4$ loading ranging from 10-40 wt.% by controlling the concentration of cobalt nitrate in the solution, and studied the intake of SBA-16_100 for $Co_3O_4$ by SEM images, Figure 6. With the increase of $Co_3O_4$ loading, the amount of $Co_3O_4$ particles staying outside the SBA-16 increases, and the maximum intake seems to be reached at 30% loading, as the amount of $Co_3O_4$ outside SBA-16 increases abruptly when the loading increases from 30% to 40%. Thus the loading of $Co_3O_4$ is controlled at 25 wt.% in this study, to avoid the formation of large amount of $Co_3O_4$ outside the template while keeps high yield, and ensure that the $Co_3O_4$ prepared is mostly replicated from the template.

In order to observe further the surface morphology of the replicated $Co_3O_4$, SEM images of $Co_3O_4$-16_80 were taken and shown in Figure 7. The large number of stacked nanoparticles indicates clearly that they are replicated from the cages of SBA-16. Interestingly, a shell assembled of small particles is also observed, like a basket (see the edge of the particles in the left

picture). A careful observation shows that hollow spheres are formed in the sample (see the right picture). From the SEM images of the $Co_3O_4$-silica composites shown in Figure 6, it is seen that there have lots of dodecahedrons and also spheres (see Figure S5), composed of SBA-16, exist. Thus we consider that the production of these hollow spheres should be related to the dodecahedral or spherical structure of SBA-16, and they are formed through the self-assemble of the $Co_3O_4$ particles, as can be seen that large amount of small particles are presented on the wall. The presence of hollow sphere is rather interesting, which means that particles can be self-assembled during the template removing process, and to the best of our knowledge, no related observation has been reported in literature.

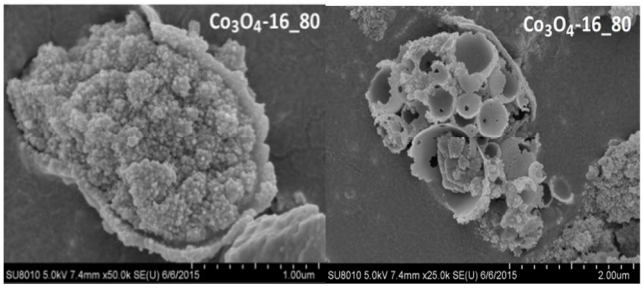


Figure 7. SEM images of the replicated $Co_3O_4$-16_80 sample

SEM images on $Co_3O_4$-16_100, $Co_3O_4$-16_120 and $Co_3O_4$-15_100 were also taken and presented in Figure S6, showing that small particles/hollow spheres are replicated from the SBA-16 template and nanowires are replicated from the SBA-15 template, in accordance to that observed in the TEM images.

### 3.3 Surface chemistries

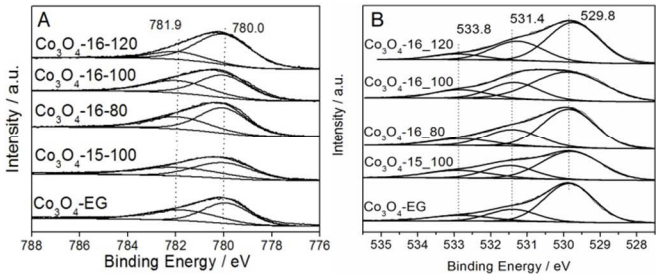


Figure 8. The Co 2p (A) and O 1s (B) XPS spectra of the $Co_3O_4$-16_T, $Co_3O_4$-15_100 and $Co_3O_4$-EG.

Figure 8 shows the Co 2p and O 1s XPS spectra of the series $Co_3O_4$ samples and the corresponding surface compositions are listed in Table 2. An overall evaluation on the molar ratio of surface Co to O (Co/O) shows that $Co_3O_4$ replicated from SBA-16 has higher Co/O ratio than that replicated from SBA-15 or that prepared by sol-gel method, due to the smaller particle size and the 3D structure of $Co_3O_4$-16_T. Thus, $Co_3O_4$-16_80 with the smallest particle size and the highest surface area has the most, and $Co_3O_4$-15_100 with the nanowire structure has the least exposed surface cobalt atoms.

For the Co 2p spectra, the peak position is in well accordance with that of $Co_3O_4$ reported in literature.[51] The asymmetrical Co 2p signal of each catalyst could be deconvoluted into two components, which are located at binding energy (BE) of 780.0 and 781.9 eV and are assigned to the $Co^{3+}$ and $Co^{2+}$ species, respectively.[52] It is known that oxides with smaller particle size have higher surface energy, more exposed metal atoms and are easier to be oxidized by oxygen in the air. Thus $Co_3O_4$-15_100 with nanowire structure and $Co_3O_4$-EG with bigger particle size has low, and $Co_3O_4$-16_80 with the smallest particle size has the largest surface $Co^{3+}/Co^{2+}$ molar ratio. It is thus expected that $Co_3O_4$-16_80 would have the strongest reducibility and may exhibit the best activity in oxidation reaction.

Table 2.XPS results of the samples

| Sample | Molar ratio determined from XPS spectra | | |
|---|---|---|---|
| | Co/O | $Co^{3+}/Co^{2+}$ | $O_{ads}/O_{latt}$ |
| $Co_3O_4$-16_120 | 0.59 | 1.44 | 0.58 |
| $Co_3O_4$-16_100 | 0.56 | 1.49 | 0.61 |
| $Co_3O_4$-16_80 | 0.51 | 1.62 | 0.63 |
| $Co_3O_4$-15_100 | 0.41 | 1.27 | 0.56 |
| $Co_3O_4$-EG | 0.43 | 1.29 | 0.48 |

For the O 1s spectra, three peaks can be fitted according to literature, which are centered at 529.8, 531.4 and 532.8 eV, and are attributed to the lattice oxygen, the chemically adsorbed oxygen and the oxygen of hydroxyl groups (or chemisorbed water), respectively.[53-55] Quantitative analysis reveals that the molar ratio of $O_{ads}/O_{latt}$ for $Co_3O_4$-EG is the lowest (0.48) and that for $Co_3O_4$-16_80 is the largest (0.63), which is in well agreement with the change observed for surface $Co^{3+}/Co^{2+}$ ratio of the samples (with an exception for $Co_3O_4$-15_100). This indicates that $Co_3O_4$-16_80 has the strongest ability to activate oxygen adsorbed on its surface, due to the high surface $Co^{3+}/Co^{2+}$ ratio.

That is, not only the surface morphology but also the surface chemistry of the replicated $Co_3O_4$ could be controlled by using a desired template. This is interesting especially in catalysis which relates intimately both to the surface morphology and to the surface chemistry of catalyst.

Because of the importance of surface chemistry of materials in catalysis, we have tried to detect the variations in surface chemistry of the $Co_3O_4$-16_T by UV-Raman spectra, Figure S7. Unfortunately, no appreciable shift, caused by the variations in surface chemistry, is observable in the spectra. This could be that the change in surface chemistry is too small to be detected by this measurement, since the samples were prepared with the same procedures. Indeed, from the $O_{ads}/O_{latt}$ ratio, which is an indication of the amount of oxygen vacancy created, detected in the XPS spectra, it is seen that only a minor change, from 0.58 to 0.63, is observed. The significantly attenuated peak intensity from $Co_3O_4$-16_80 to $Co_3O_4$-16_120 could be attributed to the increased particle size, thus fewer amounts of cobalt and oxygen responding to these peaks is exposed on the surface for $Co_3O_4$-16_120 with bigger particle size.

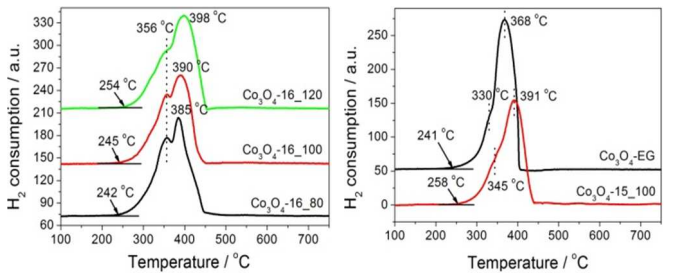


Figure 9. $H_2$-TPR profiles of the investigated $Co_3O_4$ samples

Temperature programmed reduction of hydrogen ($H_2$-TPR), which is used to measure the reducibility of materials, is further conducted, with the aim of studying the reducibility of samples, and the results are shown in Figure 9. For simplicity, the $H_2$-TPR profiles of $Co_3O_4$-16_T, and those of $Co_3O_4$-15_100 and $Co_3O_4$-EG are presented separately. A shoulder peak at 330-360 °C and a main peak at 360-390 °C (see the marks in the profile) are observed for all the samples, and they are attributed to the reduction of $Co^{3+}$ to $Co^{2+}$ and $Co^{2+}$ to metallic Co, respectively. For $Co_3O_4$-16_T, the temperature for the initial reduction of $Co^{3+}$ species and the reduction of $Co^{2+}$ to metallic Co increases from $Co_3O_4$-16_80 to $Co_3O_4$-16_100 and to $Co_3O_4$-16_120, which is in agreement with the observations in the particle size and the surface $Co^{3+}/Co^{2+}$ ratio. That is, sample with smaller particle size and higher $Co^{3+}/Co^{2+}$ ratio is easier to be reduced or has stronger reducibility. The temperature at the peak maximum of the shoulder peak, corresponding to the reduction of $Co^{3+}$ to $Co^{2+}$, is however almost the same (356°C) for the three samples. In general, the $Co_3O_4$-16_80 with the strongest reducibility should exhibit the lowest reduction temperature. The similar reduction temperature could be that the reduction temperature of $Co_3O_4$-16_80 is delayed because of the high percentage of $Co^{3+}$ species or the more amount of hydrogen consumed, as documented previously.[56]

Similarly, the temperature at the peak maximum of the shoulder peak for $Co_3O_4$-16_EG and $Co_3O_4$-15_100 shifts to a further lower position because of the decreased percentage of $Co^{3+}$ species. Yet it is noted that the $Co_3O_4$-16_EG sample shows always the lowest reduction temperature either for the initial reduction of $Co^{3+}$ species, the reduction of $Co^{3+}$ to $Co^{2+}$, or the reduction of $Co^{2+}$ to metallic Co. This might be relevant to the fact that this sample is not prepared by templating method and has not been treated by NaOH in aqueous solution. Thus for the replicated $Co_3O_4$-n_T, there might have a trace amount of silica, yielded from the template etching process, remained on the surface, restraining the reduction.

To support the above conclusions that the particle size of $Co_3O_4$-16_T increases and the reducibility decreases with the hydrothermal temperature of SBA-16_T, and exclude possible influences resulted from the template etching process, we measured the $H_2$ adsorption capacity and the dispersion of metallic cobalt supported on SBA-16 (defined as Co/SBA-16), which was obtained by direct reduction of $Co_3O_4$/SBA-16_T with $H_2$ at 350 °C, and the results are listed in Table S1. Both the amount of hydrogen desorbed and the dispersion of metallic cobalt decrease with the hydrothermal temperature of SBA-16_T, indicating a decreased reducibility and an increased particle size. Because the metallic cobalt was obtained directly from the $Co_3O_4$, thus the trend obtained from the Co/SBA-16 could be a reflection of the $Co_3O_4$/SBA-16. That is, the particle size and thus the reducibility of $Co_3O_4$ formed on SBA-16 indeed depend on the pore size of SBA-16. This supports well the phenomena observed from the replicated $Co_3O_4$-16_T.

### 3.4 Catalytic performances

Catalytic performances of the series $Co_3O_4$ samples are tested by CO oxidation reaction, which is a major route of removing toxic CO in exhaust gas and is one of the mostly used model reaction in heterogeneous catalysis. Figure 10 presents the CO conversion obtained from the catalysts at temperature range of 70 - 150 °C, showing that they are all active for the reaction and 100% CO conversion can be obtained at 150 °C. Detailed investigations show, however, that differences in the activities of the catalysts at temperature below 150 °C exist, and the activity decreases in order of $Co_3O_4$-16_80 > $Co_3O_4$-16_100 > $Co_3O_4$-16_120 > $Co_3O_4$-15_100 > $Co_3O_4$-EG, which fits well to the conclusions obtained above. That is, $Co_3O_4$-16_80 with the smallest particle size, largest surface area, highest surface $Co^{3+}/Co^{2+}$ molar ratio and strongest reducibility exhibits the best CO oxidation activity. The template of sample with small particle size is thus suggested if the material is to be used for catalysis. Catalytic performances of other metal oxides, replicated from SBA-15_100, for CO oxidation are also tested, showing they are active for the reaction, with the best activity obtained from $Ce_{0.7}Cu_{0.3}O_2$ (see Figure S8).

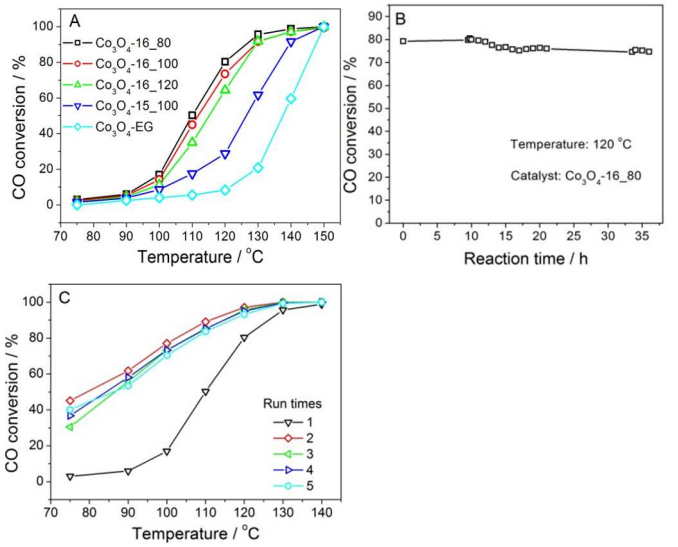


Figure 10. (A) CO oxidation conversion obtained from $Co_3O_4$ prepared with different templates or methods; (B) Stability of $Co_3O_4$-16_80 for CO oxidation conducted at 120 °C. Reaction conditions: 50 mg catalyst; 0.5% CO-7.5% $O_2$/Ar, flow rate of 50 mL $min^{-1}$

The long-term stability of $Co_3O_4$-16_80 for CO oxidation is further conducted to see if the material has good stability for catalysis use. Results in Figure 10B show that the catalyst is stable in the reaction, with less than 6% decrease in the activity after working on stream at 120 °C for 36 h. Characterizations by XRD and TEM for the used $Co_3O_4$-16_80 (after the stability test) shows that only a slight change in the crystalline size, from 16.1 to 16.6 nm, is observed and the mesoporous structure is preserved, see the picture of $Co_3O_4$-16_80-Used presented in Figure 2 and Figure 4F, respectively, confirming further that the $Co_3O_4$-16_80 is stable in the reaction.

Besides the long-term stability, we also tested the reusability of $Co_3O_4$-16_80 for the reaction, and the results are shown in Figure 10C. It is observed that the activity was significantly increased after the first run, especially at low temperature range, which could be due to the reason that the catalyst was activated after the first run. Indeed, we found that the CO oxidation activity was significantly improved after a pre-treatment procedure on the catalyst, Figure S9. In previous work it was reported that the pre-treatment of $Co_3O_4$ is an important step of improving the CO oxidation activity,[57] supporting our findings. The activity keeps similar after the second run and only a slight variation is observed. Considering that the catalyst is stable in the reaction (see Figure 10B) and the random changes in activity between the third and fifth runs, it is suggested that the change is attributed to an experimental error. The similar activity obtained from different runs suggests again that the material has good stability during the reaction.

In the end, we compared the CO oxidation activities of the materials with that reported in literature, to see the difference between them, Table S2. In general, the materials synthesized here needs higher temperature for CO ignition and complete oxidation, which could be partly due to the fewer amount of catalyst used (50 mg vs. 200 mg, for example [36]) and the fact that our catalysts were not pre-treated at high temperature, which is reported to be a crucial factor influencing the low-temperature CO oxidation activity.[57] However, the herein materials showed better stability to the reaction (see Figure 10B and 10C) than that reported in literature (see for example reference 36, where a decrease of 85% to 43% in CO conversion was observed after running for 4 h, and reference 6, where the CO conversion decreased to zero after 12 h). We thus consider that the herein reported materials would have great application in practical use, because of their high thermal stability as well as the mediate temperature (ca. 130 °C) for complete oxidation, since in most industrial plants the temperature of CO containing exhaust is above 130 °C, thus ensuring the complete removal of CO.

## 4. Conclusions

Metal oxides with expected structure and surface morphologies are replicated from the shaped templates (SBA-16 and SBA-15) via an incipient wetness impregnation route. Because of the variations in particle size and surface morphology, the metal oxides exhibit different surface properties, leading to variations in catalytic performances. This suggests that surface property of metal oxides can be controlled by using a designed template, to some extent. In case of $Co_3O_4$, sample with three-dimensionally mesoporous structure and two-dimensionally channel structure can be replicated from SBA-16 and SBA-15, respectively, and the particle size and pore size of $Co_3O_4$ can be controlled by varying the hydrothermal temperature of the template. Further studies indicate that the $Co_3O_4$-16_80 with the smallest particle size and the largest surface area possesses the strongest reducibility, thus leading to the best catalytic performances for CO oxidation reaction. This material is also highly stable in the reaction, with no appreciable change in the activity observable between the first and second run, and less than 6% loss in the activity after running on stream at 120 °C for 36 h.

## Acknowledgements

Finance support from the National Science Foundation of China (21203253, 21203254), the Natural Science Foundation of Hubei Province of China (2015CFA138), the Science and Technology Activities of Overseas Personnel Preferential Funding Project (BZY14038), the Natural Science Fundation of South-Central Univeristy for Nationalities (XTZ15016) and the open project of the Functional Inorganic Materials Chemistry of the Key Laboratory of Ministry of Education, Heilongjiang University, is gratefully acknowledged.

## Notes and references

Key Laboratory of Catalysis and Materials Science of the State Ethnic Affairs & Commission Ministry of Education, South-Central University for Nationalities, Wuhan 430074, China

* Corresponding author. E-mail: ciaczjj@gmail.com (J. Zhu); zhaoyanxi@126.com (Y. Zhao)

Electronic Supplementary Information (ESI) available: Data obtained from $H_2$-TPD; Comparison of activity with that in literature; Small-angle XRD patterns; $N_2$ physisorption isotherms; TEM and SEM images; UV-Raman spectra and CO oxidation activity of other metals NiO, $CeO_2$ and $Ce_{0.7}Cu_{0.3}O_2$, were supplied in the supplementary material. See DOI: 10.1039/b000000x/

1 C.T. Kresge, M.E. Leonowicz, W.J. Roth, J.C. Vartuli, J.S. Beck, *Nature*, 1992, **359**, 710.
2 A.S. Poyraz, S. Biswas, H.C. Genuino, S. Dharmarathna, C.-H. Kuo, S.L. Suib, *ChemCatChem*, 2013, **5**,920.
3 D.E. De Vos, M. Dams, B.F. Sels, P.A. Jacobs, *Chem. Rev.*, 2002, **102** , 3615.
4 Z. Wu, D. Zhao, *Chem.Commun.*, 2011, **47**, 3332.
5 F. Schüth, *Chem. Mater.*, 2001, **13**, 3184.
6 W. Song, A.S. Poyraz, Y. Meng, Z. Ren, S.Y. Chen, S.L. Suib, *Chem. Mater.*, 2014, **26**, 4629.
7 R. Ryoo, S.H. Joo, M. Kruk, M. Jaroniec, *Adv. Mater.*, 2001, **13**,677.
8 F. Jiao, A. Harrison, J.-C. Jumas, A.V. Chadwick, W. Kockelmann, P.G. Bruce, *J. Am. Chem. Soc.*, 2006, **128**, 5468.
9 B. Tian, X. Liu, H. Yang, S. Xie, C. Yu, B. Tu, D. Zhao, *Adv. Mater.*, 2003, **15**, 1370.
10 C. Dickinson, W. Zhou, R.P. Hodgkins, Shi, Zhao, He, *Chem. Mater.*, 2006, **18**, 3088.
11 A. Rumplecker, F. Kleitz, E.-L. Salabas, F. Schüth, *Chem. Mater.*, 2007, **19**, 485.
12 F. Jiao, P.G. Bruce, *Adv. Mater.*,2007, **19**, 657.
13 F. Jiao, A.H. Hill, A. Harrison, A. Berko, A.V. Chadwick, P.G. Bruce, *J. Am. Chem. Soc.*, 2008, **130**, 5262.
14 Y. Wang, C.M. Yang, W. Schmidt, B. Spliethoff, E. Bill, F. Schüth, *Adv. Mater.*, 2005, **17**, 53.
15 S.C. Laha, R. Ryoo, *Chem. Commun.*, 2003, **17**, 2138
16 M. Imperor-Clerc, D. Bazin, M.-D. Appay, P. Beaunier, A. Davidson, *Chem. Mater.*, 2004, **16**, 1813.
17 S. Sun, Q. Gao, H. Wang, J. Zhu, H. Guo, *Appl. Catal. B-Environ.*, 2010, **97**, 284.
18 W. Yue, W. Zhou, *Chem. Mater.*, 2007, **19**, 2359.
19 W. Yue, A.H. Hill, A. Harrison, W. Zhou, *Chem. Commun.*, 2007, 2518.
20 Y. Xia, H. Dai, H. Jiang, L. Zhang, *Catal. Commun.*, 2010, **11**, 1171.
21 H. Yen, Y. Seo, R. Guillet-Nicolas, S. Kaliaguine, F. Kleitz, *Chem. Commun.*, 2011, **47**, 10473.
22 H. Yen, Y. Seo, S. Kaliaguine, F. Kleitz, *Angew. Chem. Int. Ed.*, 2012, **51**, 12032.
23 J. Deng, L. Zhang, H. Dai, Y. Xia, H. Jiang, H. Zhang, H. He, *J. Phys. Chem. C*, 2010,**114**, 2694.
24 P. Thormählen, M. Skoglundh, E. Fridell, B. Andersson, *J. Catal.*, 1999, **188**, 300.
25 M. Cargnello, C. Gentilini, T. Montini, E. Fonda, S. Mehraeen, M. Chi, M. Herrera-Collado, N.D. Browning, S. Polizzi, L. Pasquato, P. Fornasiero, *Chem. Mater.*, 2010, **22**, 4335.
26 H. Yamaura, K. Moriya, N. Miura, N. Yamazoe, *Sensor. Actuat. B-Chem.*, 2000, **65**, 39.
27 S.H. Taylor, C. Rhodes, *Catal. Lett.*, 2005, **101**, 31.
28 C.-B. Wang, C.-W. Tang, S.-J. Gau, S.-H. Chien, *Catal. Lett.*, 2005, **101**, 59.

29 A. Holmgren, B. Andersson, D. Duprez, *Appl. Catal. B-Environ.*, 1991, **22**, 215.
30 H. Zhu, Z. Qin, W. Shan, W. Shen, J. Wang, *J. Catal.*, 2005,**233**, 41.
31 M.-F. Luo, J.-M. Ma, J.-Q. Lu, Y.-P. Song, Y.-J. Wang, *J. Catal.*, 2007, **246**, 52.
32 L. Hu, Q. Peng, Y. Li, *J. Am. Chem. Soc.*, 2008, **130**, 16136.
33 T. He, D. Chen, X. Jiao, Y. Xu, Y. Gu, *Langmuir*, 2004, **20**, 8404.
34 B.B. Lakshmi, C.J. Patrissi, C.R. Martin, *Chem. Mater.*, 1997, **9**, 2544.
35 J. Feng, H.C. Zeng, *Chem. Mater.*, 2003, **15**, 2829.
36 H. Tüysüz, M. Comotti, F. Schüth, *Chem. Commun.*, 2008, **34**, 4022.
37 C. Baatz, U. Prüße, *J. Catal.*, 2007, **249**, 34.
38 J. Zhu, T. Wang, X. Xu, P. Xiao, J. Li, *Appl. Catal. B: Environ.*, 2013, **130-131**, 197.
39 P. Xiao, Y. Zhao, T. Wang, Y. Zhan, H. Wang, J. Li, A. Thomas, J. Zhu, *Chem. Eur. J.*, 2014, **20**, 2872.
40 H. Xiong, Y. Zhang, S. Wang, J. Li, *Catal. Commun.*, 2005, **6** , 512.
41 J.R.A. Sietsma, J.D. Meeldijk, J.P. den Breejen, M. Versluijs-Helder, A.J. van Dillen, P.E. de Jongh, K.P. de Jong, *Angew. Chem. Int. Ed.*, 2007, **119** , 4631.
42 P. Azadi, R. Farnood, E. Meier, *J. Phys. Chem. A*, 2009, **114**, 3962.
43 D. Zhao, J. Feng, Q.Huo, N. Melosh, G. H.Fredrickson, B. F. Chmelka, G. D. Stucky, *Science*, 1998, **279**, 548.
44 J. Zhu, K. Kailasam, X. Xie, R. Schomaecker, A. Thomas, *Chem. Mater.*, 2011, **23**, 2062.
45 Y. Zhao, Y. Zhang, J. Chen, J. Li, K. Liew, M.R.B. Nordin, *ChemCatChem*, 2012, **4**, 265.
46 L. Zhong, F. Hai, P. Xiao, J. Hong, J. Zhu, *RSC Adv.*, 2014, **4**, 61476.
47 P. Van Der Voort, M. Benjelloun, E.F. Vansant, *J. Phys. Chem. B*, 2002, **106**, 9027.
48 T.W. Kim, R. Ryoo, M. Kruk, K.P. Gierszal, M. Jaroniec, S. Kamiya, O. Terasaki, *J. Phys. Chem. B*, 2004, **108**, 11480.
49 H. Sugimura, A. Hozumi, T. Kameyama, O. Takai, *Adv. Mater.*, 2001, **13**, 667.
50 P. Xiao, J. Hong, T. Wang, X. Xu, Y. Yuan, J. Li, J. Zhu, *Catal. Lett.*, 2013, **143**, 887.
51 J. Zhu, K. Kailasam, A. Fischer, A. Thomas, *ACS Catal.*, 2011, **1**, 342.
52 C. Schenck, J. Dillard, J. Murray, *J. Colloid Interface Sci.*, 1983, **95**, 398.
53 C. Yuan, L. Yang, L. Hou, L. Shen, F. Zhang, D. Li, X. Zhang, *J. Mater. Chem.*, 2011, **21**, 18183.
54 D. Briggs, JC Riviere in: Practical Surface Analysis. Eds. D. Briggs and MP Shah, in, Wiley, London, 1983.
55 M.M. Natile, A. Glisenti, *Chem. Mater.*, 2002, **14**, 3090.
56 J. Zhu, H. Li, L. Zhong, P. Xiao, X. Xu, X. Yang, Z. Zhao, J. Li, *ACS Catal.*, 2014, **4**, 2917.
57 Y. Ren, Z. Ma, L.P. Qian, S. Dai, H.Y. He, P.G. Bruce, *Catal. Lett.*, 2009, **131**, 146

## Graphical Abstract

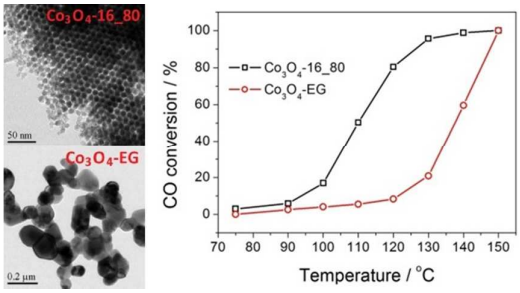


$Co_3O_4$ templated from mesoporous silica show stable and better activity for CO oxidation than that synthesized by traditional sol-gel method.